Understanding subsalt illumination through ray-trace modeling, Part 2: Dipping salt bodies, salt peaks, and nonreciprocity of subsalt amplitude response

David Muerdter, Diamond Geophysical Research, Redmond, Washington, U.S.
Mike Kelly, Diamond Geophysical Research, Dayton, Montana, U.S.
Davis Ratcliff, Diamond Geophysical, Houston, Texas, U.S.

The interest in subsalt imaging has been fueled by numerous discoveries beneath salt in the Gulf of Mexico in the last decade. A most effective tool in making these discoveries is 3-D prestack depth migration (PreSDM), which allows imaging of reflectors under the salt sheets and of detached bodies of irregular shape. Ray-trace modeling can simulate seismic illumination problems such as shadow zones or seismic focusing and allow better interpretation of subsalt seismic data.

The modeling process involves building a computer model that includes salt shapes and velocity variations, simulating an entire 3-D seismic survey with ray-trace modeling, and sorting the data into common reflection point (CRP) gathers. Plots and maps of the fold and especially the amplitude on the reflecting horizons are compared with the real seismic data to better understand the illumination complexities.

In the first part of this three-part article (*TLE*, June 2001), the theory and methods of ray-trace modeling were discussed and simple 2-D models were ray-traced to investigate the effects of salt edges. In this paper illumination beneath dipping salt bodies is examined, lack of amplitude reciprocity beneath dipping salt is reported, and the effects of peaks and pits in salt bodies are studied. The Hickory discovery area in Grand Isle South block 116 is shown to have an amplitude anomaly produced by focusing through a salt

Table 1. Maximum reflection angle for flat salt slab models with various thickness of salt. Top of salt and depth of reflector remain constant

Salt thickness	Max reflection angle	
	No salt	Subsalt
250 m	35.6°	30.5°
1000 m	35.6°	26.3°
1500 m	35.6°	24.4°

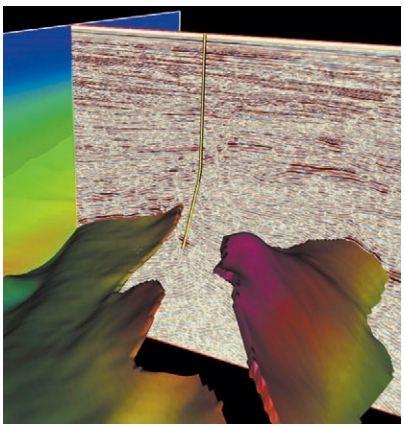

Figure 1. 3-D visualization of the relatively thin dipping salt slabs in the Tanzanite discovery area in Eugene Island Block 346. View is from the southeast. Salt slabs are color coded by depth (red = shallow, blue = deep). A section from the 3-D PreSDM volume is shown behind the well. To the left (west) the seismic section intersects a translucent velocity section from the 3-D velocity volume (blue = low velocity, red = high).

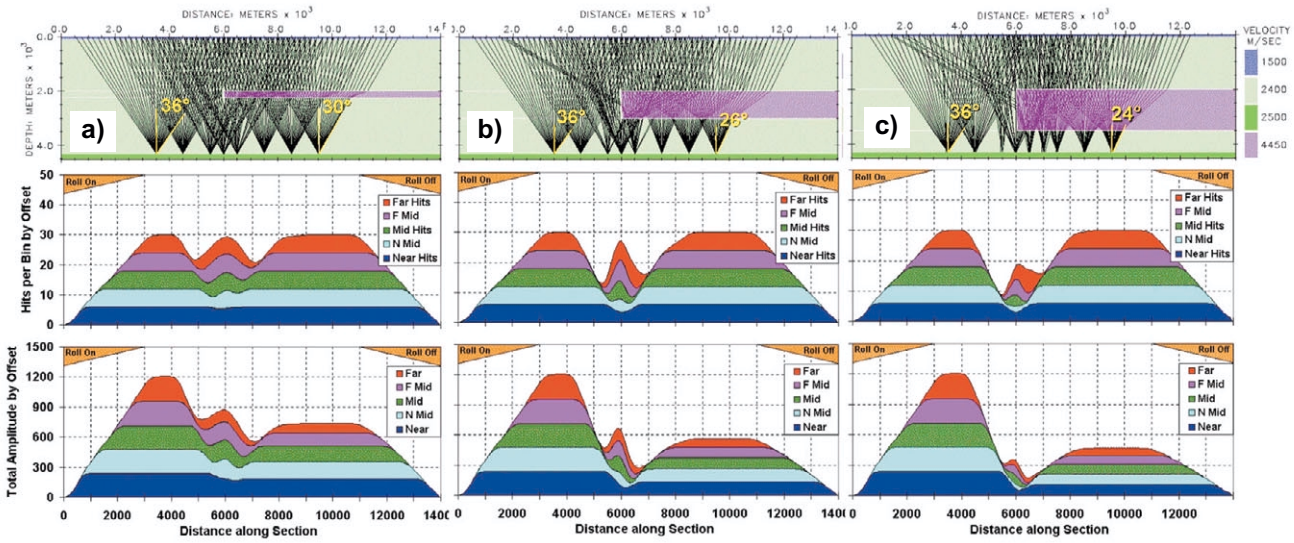

Figure 2. Raypaths for selected CRP gathers and CRP fold and amplitude results. The flat salt slabs in the models vary in thickness: (a) 250 m thick, (b) 1000 m thick, and (c) 1500 m thick.

Table 2. Rock properties used in model and in independent calculations

	Vp	Vs	Density
Water	1500 m/s	1 m/s	1.030 gm/cm^3
Sediments	2400 m/s	900 m/s	2.166 gm/cm^3
Salt	4450 m/s	2250 m/s	2.050 gm/cm^3

peak. The third and final part of this series examines the effects of salt ridges and salt furrows, including the effects of acquisition direction relative to the structural orientation.

By limiting the number of variables, ray tracing of simple seismic models can isolate and investigate individual structural and velocity variables. Ray-trace results from simple models are then analyzed to ascertain the subsalt illumination produced by various salt structures. Analogous examples from the Gulf of Mexico show similar effects in more complex real-world models. Observations and conclusions of the modeling results are summarized at the end of each section. Part 3 of this paper will recap the conclusions.

Dipping slabs. While some salt sheets in the Gulf of Mexico are flat, many are inclined such as the dipping salt sheet at Tanzanite Field in Eugene Island Block 346 (Figure 1). Therefore, simple models were built with inclined salt slabs. The models were similar to the salt-edge models discussed in Part 1, but the inclined models have only one type of salt edge—one perpendicular to the top and base of salt. This edge is like the near-vertical salt edge in Figure 2. Two different thicknesses of salt were modeled, 250 m and 1000 m, compared to the 1500-m thick salt in the edge models. The top of salt had a minimum depth of 2000 m. The reflector was at 4300 m and salt slab dip varied from 10-50°. A flat salt slab also was

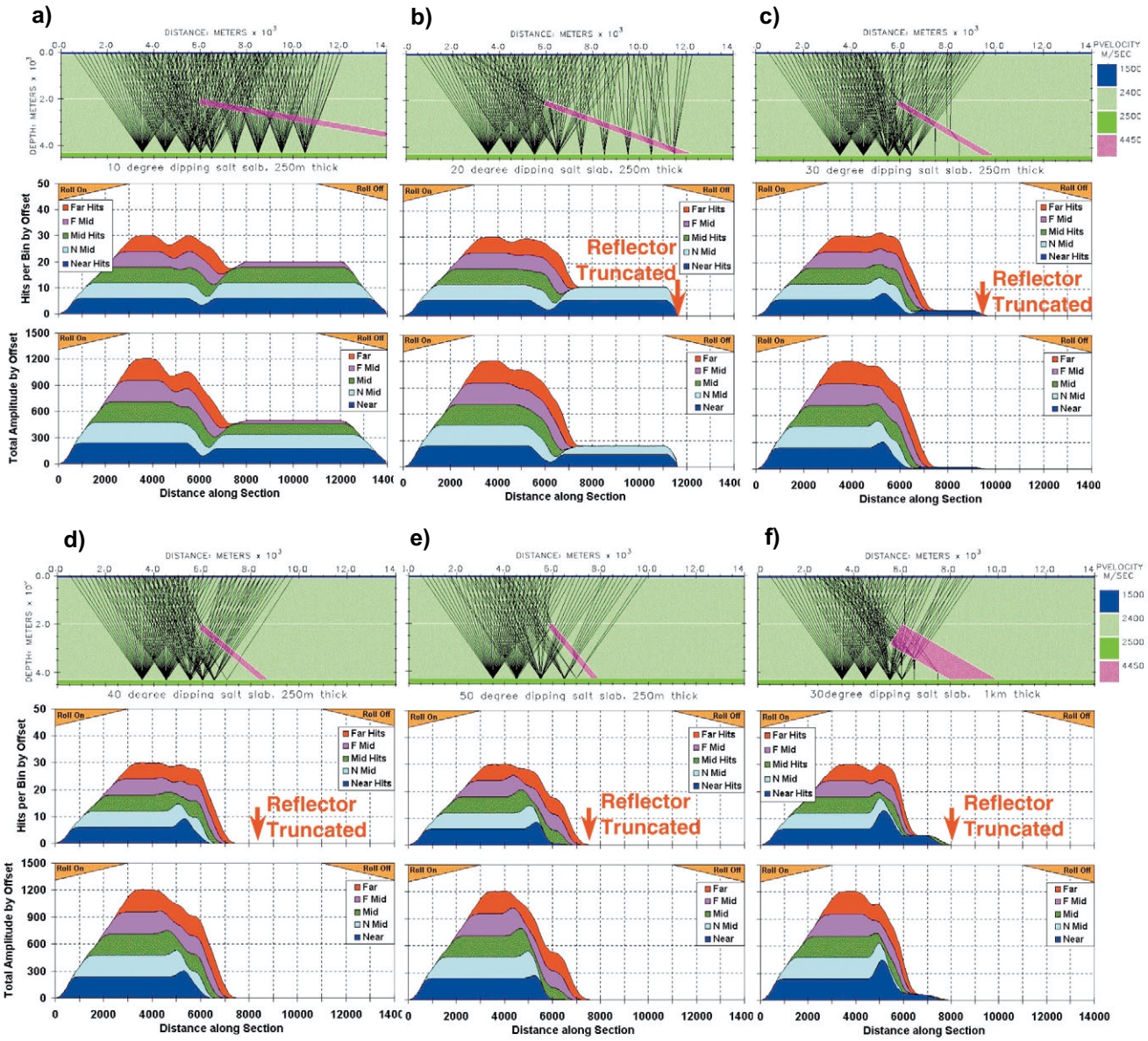

Figure 3. (a) to (e) Models with 250-m thick dipping salt slab on one side of model and no salt on the other. Salt edge is perpendicular to top and base of slab. Models differ by dip of slab (10°, 20°, 30°, 40°, and 50°). Model is overlain with selected RPG raypaths and shown above the RPG hits per bin and total amplitude per bin plots. (f) 30° dipping salt slab 1-km thick. Note the larger influence of rays penetrating the perpendicular edge of salt in the thicker salt slab.

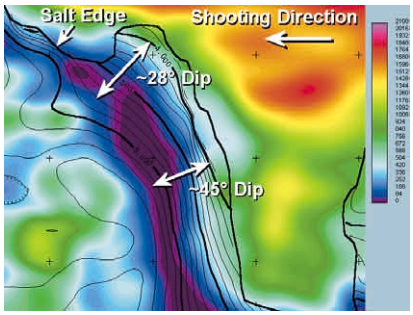

Figure 4. Map of CRP amplitude illumination of a subsalt horizon in Tanzanite area. The amplitude is color coded (blue = low amplitude to red = high). The contours of the base of salt are overlain and the edge of salt marked with bold black line. Note the shadow zone about 1500m inside the edge of the dipping salt. Note that the illumination increases slightly when the dip decreases below the critical angle of 32°. The illumination increases as the salt slab flattens in the southwest.

Table 3. Transmission coefficients at the various interfaces for a ray with 5400 m offset as shown as red line in Figure 6a*

	Water bottom 21.78°-36.41°	Sed-salt 16.41°-31.59°	Salt-sed 51.59°-25.00°	Water bottom 25.00°-15.32°	Transmission product
Downdip	0.475	0.750	0.991	1.469	0.519
Updip	1.385	1.170	0.823	0.465	0.620

*Zoeppritz equations were used in the calculations

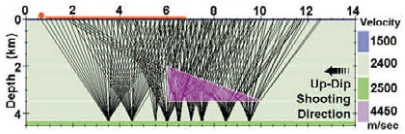

Figure 5. A model of a salt body with a 20° dipping top surface is ray traced using a simulated 6000-m marine cable trailing 200 m behind a source. The position of the cable (red line) is shown for a shot (red circle) 600 m along the line. Two seismic lines were shot over the model, one from left to right (termed downdip) and one from right to left (updip). Selected CRP gathers are shown on plot of the model for the updip line.

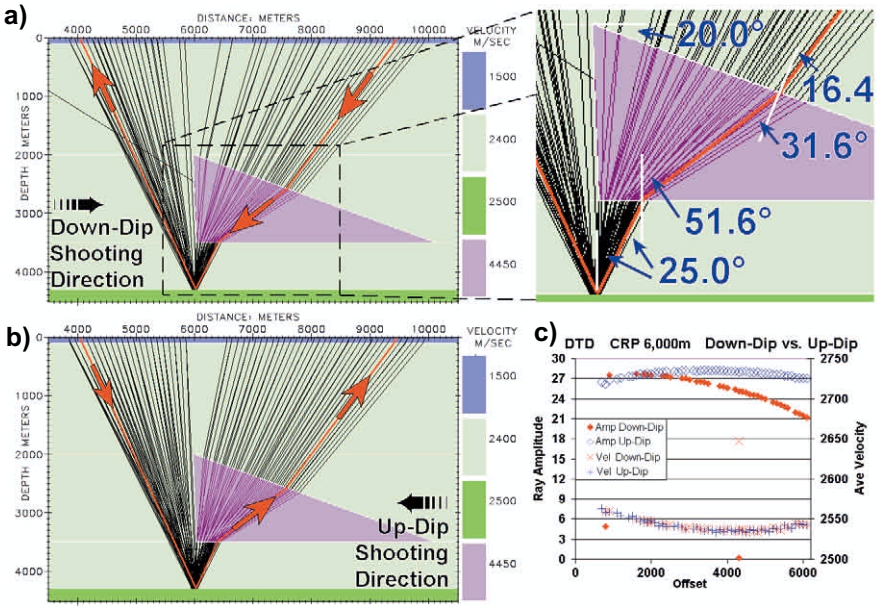

Figure 6. (a) Plot of all rays in CRP bin centered at 6000 m for a 2-D line shot downdip. An enlargement of the salt body is shown to the right with angle of incidence and refraction shown for a ray with 5400-m offset. Amplitudes of rays in both directions along a raypath marked in red are manually calculated in the text. (b) Plot of all rays in CRP bin at 6000 m for a 2-D line shot from right to left with exact same shot locations as (a). (c) Comparison of amplitude results of lines shot in opposite directions. The amplitude asymmetry is shown by the downdip line (red diamonds) being less than the amplitude of the updip line (blue open diamonds). The difference increases with offset. The rays have the same travel path as confirmed by the average velocity (distance/traveltime) for the rays being the same. Note that the updip shooting direction has a few more near-offset rays captured.

modeled for comparison.

The flat salt slab models allow effects of different salt thicknesses to be assessed. Figure 2a shows that the maximum reflection angle is reduced from 36° to 30° for the 250-m slab. A list of maximum reflection angles for the different thicknesses of salt (Table 1) indicates that the reflection angle decreases as salt thickness increases. Also note the edge of salt on the thin slab is less disruptive than the thicker salt slab (Figures 2a-c).

Figure 3 contains the raypath and CRP results for the dipping 250-m salt slab. The illumination problems are similar for the dipping 1000-m slab; therefore, only the 30° dip case for the 1000-m slab is shown in Figure 3f.

For dipping salt slabs, subsalt illumination response falls into two categories: dip below critical angle and dip above critical angle. For the rock properties in these models, the critical angle at the sediment-salt interface is 32.6°. For a salt slab with dip less than critical angle, some energy will transmit through the salt (Figures 3a-c). As dip increases, the larger offsets that strike the salt at angles beyond critical do not pass through. Note how all rays out to the full offset of 6100 m transmit through the salt on the flat salt slab (Figure 2a). But as the slab dip angle increases, the larger offsets are eliminated on the 10° dip, the 20° dip, and only the nearest offsets get through the salt at 30° dip (Figure 3c). For dips higher than the critical angles, no rays transmit through the top of salt twice (e.g., Figure 3d between 7200 and 8200 m). In all models, there is some subsalt imaging under the edge of salt where the energy travels only once through the salt (e.g., Figure 3e between 6000 and 7400 m). A prominent difference in the thicker salt slab results is the larger influence of rays penetrating the perpendicular edge of the slab (Figure 3f).

In these simple 2-D models, the top and base of salt were planar, the edge of salt perpendicular to the top and base, and the velocities in each layer constant. Real-world salt is usually much more complex and a simple critical angle calculation may be too simplistic. Therefore if the salt structure is complex or if the velocity has large lateral variations, modeling of the particular structure may be needed. For complex structures, 3-D ray tracing should use an array similar to the actual shooting geometry.

Table 4. Comparison of independent calculations and ray-trace modeling results show <0.2% difference that is within round-off error

	Independent calculations		Ray-trace model results	
	Amplitude	Relative amp	Amplitude	Relative amp
Downdip	0.519	0.836	23.135	0.838
Updip	0.620	1.000	27.614	1.000

Figure 7. (a) Plot of all rays in CRP bin centered at 8500 m for the line shot downdip. (b) Plot of all rays in CRP bin at 8500 m for the updip line with same shot locations as the downdip line. (c) Comparison of amplitude results of shooting in opposite directions. Amplitude asymmetry is shown with downdip line (red diamonds) being always less than amplitude of updip line (open blue diamonds). The rays have the same travel path as confirmed by the average velocity (distance/traveltime) for the rays being the same. Note that the reverse shooting direction has a few less far-offset rays captured.

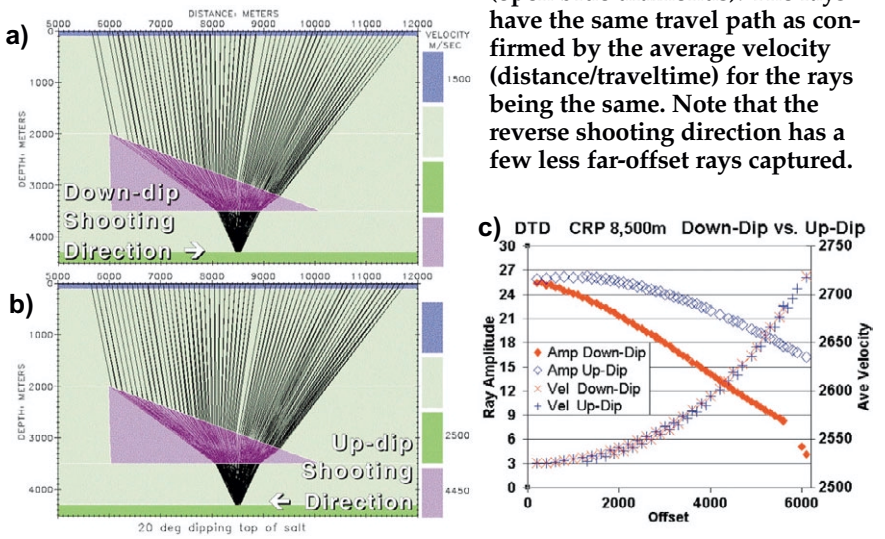

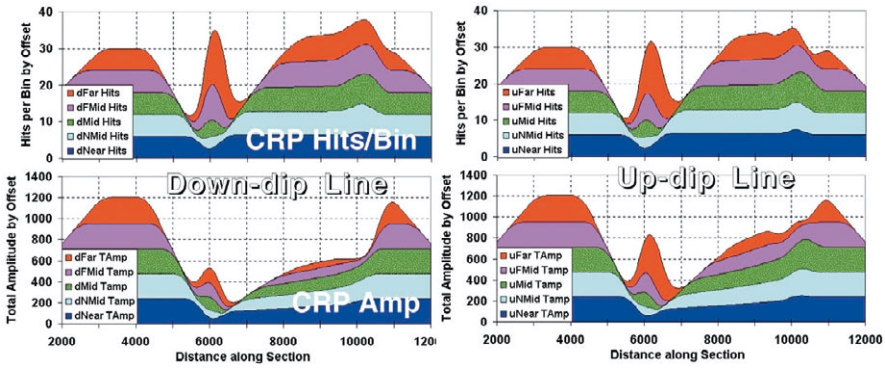

Figure 8. CRP results color coded by offset bands (blue = near offsets, red = far offsets) for downdip line (left) and updip line (right). Note that the larger offsets are greatly diminished between 7000 and 8000 m along the section.

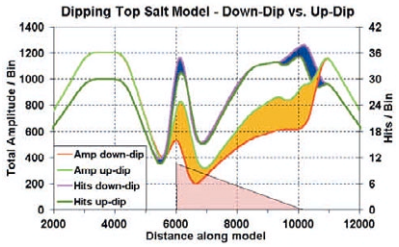

Figure 9. Comparison of CRP fold and amplitude results for downdip and updip lines. The shape and position of the salt body (pink triangle) is overlain at base of plot. Amplitude of the updip line is always greater than the downdip line (orange). As discussed in the text and shown in Figures 6 and 7, large offsets have the greatest difference in amplitude. Decrease in amplitude difference around 7000 m can then be attributed to the decrease in far-offset rays as noted in Figure 8. Under the edges of salt, downdip hits per bin is greater than in the updip line. The resultant minor amplitude difference is attributed to the ray-tracing methodology.

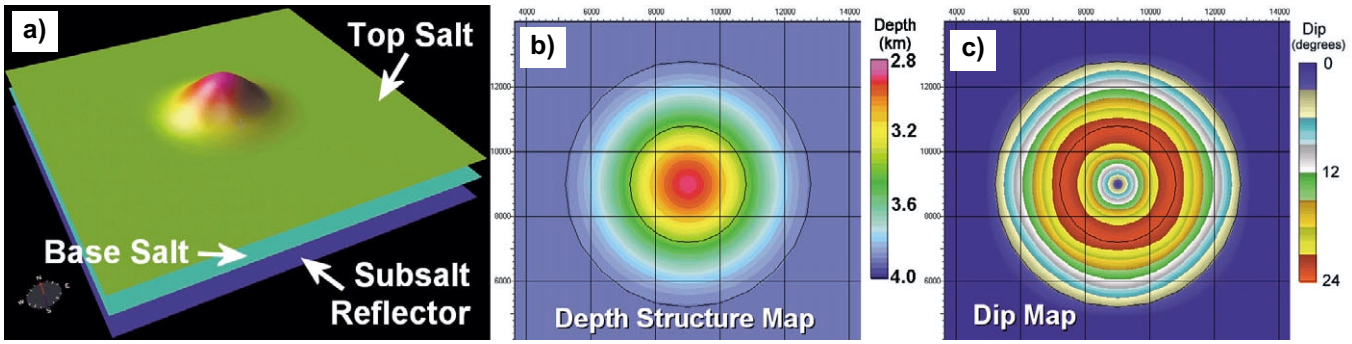

Figure 10. (a) Visualization of peak on top of salt. The peaks varied in height from 250 m to 2 km and the width at the base from 3 to 6 km. (b) Color-coded structure map of top of salt showing actual dimensions of 1 × 6 km peak. (c) Dip map on top salt surface for 1 × 6 km peak model. Note grid smoothing used to create the shape imparted a slight noncircular pattern.

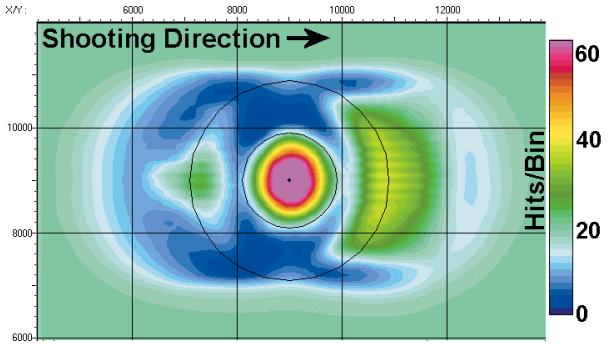

Figure 11. Fold coverage map of reflection point gathers on a flat 6200-m horizon in a 3-D survey shot from west to east over a 2-km high, >3-km wide salt peak model. The top of the flat salt slab is at 3900 m and the base at 5000 m. Results were Fresnel-zone smoothed. Note very high hits/bin peak under the salt peak.

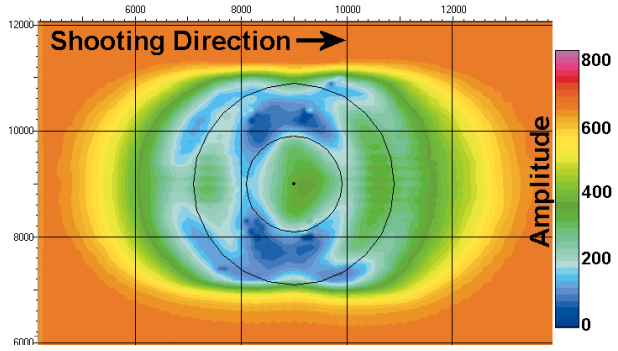

Figure 12. Reflection point gather amplitude/bin map from a flat 6200-m horizon in a 3-D survey over a 2-km high, 3-km wide salt peak model. Results were Fresnel-zone smoothed. Note that the maximum amplitude under the peak is less than the amplitude under the undeformed flat slab.

Observations from dipping slab modeling include:

- Thin salt slabs are less disruptive to imaging than thicker slabs.
- Maximum angle of reflection decreases with increased thickness of salt.
- For dipping salt, the illumination decreases as the dip increases. The larger offsets that strike the salt at greater than the critical angle are eliminated. When the salt dips more than critical angle, the area below is shadowed from rays that pass through the salt twice.
- Imaging under the edge of salt can occur by rays passing only once through salt and through sediments outside of the salt body on the other half of its reflected path.
- In a complex structural area, full-offset 3-D ray tracing may be necessary to understand the illumination problems.

For a real-world situation, consider the thin salt slabs in the area of the Tanzanite subsalt discovery in Eugene Island South block 346 in the Gulf of Mexico. Figure 1 is a 3-D visualization of the well bore deviating under the edge of salt to penetrate the high-amplitude target. The seismic section in Figure 1 has a strong amplitude anomaly associated with the reservoir just under the edge of the dipping salt sheet. This is consistent with simple models that show the area immediately under the salt edge (Figure 3d, from 6000 to 6500m) are only partially shadowed, so amplitude anomalies can be visible. Further under the salt the shadowing increases (Figure 3d, from 7000 to 8300m where the reflector pinches out against the salt).

The CRP amplitude results for reflections from a subsalt horizon (Figure 4) were created by a 3-D survey simulated over a computer model of the Tanzanite area. This Tanzanite model included a complex salt shape and lateral and vertical velocity variations. The area containing the amplitude anomaly just under the salt is adequately illuminated. But a shadow zone is seen centered about 1500 m inside the salt edge. This result is consistent with the shadowing in the dipping salt slab model that is seen in Figure 3d.

Dipping top of salt: amplitude nonreciprocity. A basic tenant of geophysics is the reciprocity principle, defined in Sheriff's *Encyclopedic Dictionary of Exploration Geophysics* as: "The seismic trace from a source at A to a geophone at B is the same as from a source at B to a geophone at A if sources and receivers are similarly coupled to the earth." This is a good approximation when dip is low or when acoustic contrasts are low. But a dipping, high-acoustic contrast interface such as with salt bodies in the Gulf of Mexico can produce large differences in subsalt reflection amplitudes for energy traveling in opposite directions along the same raypath. The variations are mainly produced because more or less energy is mode converted at the interfaces dependent on incidence angle.

After puzzling over asymmetric response of lines shot in opposite directions over a symmetrical model, a simple model was made to investigate the phenomenon. The model

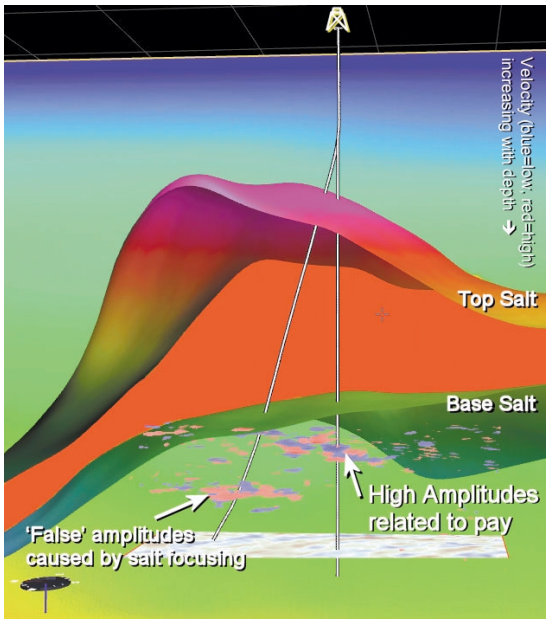

Figure 13. 3-D visualization of Hickory discovery in Grand Isle South 116. The top and base of salt are shown, along with wells, a small patch of a seismic depth slice, and clouds showing the locations of the highest seismic amplitudes. The subsalt amplitudes penetrated by the straight well represent a tested discovery. But the deeper amplitude penetrated by the deviated well proved to be a "false" HCI. 3-D ray-trace modeling predicted correctly the false bright spot before the wells were drilled (Muerdter et al., 1998).

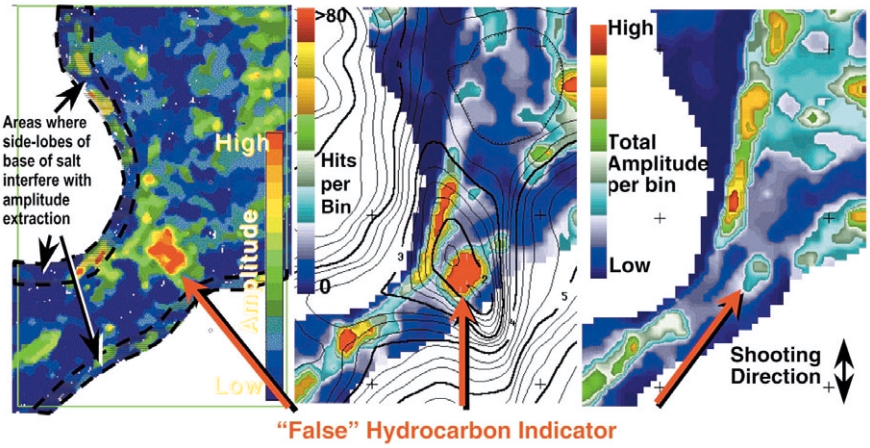

Figure 14. (a) Seismic amplitude extracted along a subsalt horizon in the Hickory discovery area (Grand Isle 116). (b) Hits per bin map for reflections from a subsalt reflector. Hits per bin values are color coded (blue = low, red = high). White areas are where the horizon truncates against base of salt. Top of salt shape is indicated by the black contours. High fold anomaly near the center of the figure indicates focusing of raypaths under the salt peak. (c) Total amplitude map showing amplitude anomaly in same location, but not as pronounced as in the fold map.

consisted of a shallow water bottom and a flat-bottomed salt body with the top of salt dipping at 20° (Figure 5). Full-offset 2-D seismic lines were simulated across the salt model in both the left to right direction (referred to as downdip in this paper) and right to left (updip). The acquisition geometry emulated a marine survey with a single 6-km long hydrophone cable and a 200-m offset from the source to the middle of the nearest receiver array. Source locations were duplicated for both forward- and reverse-simulated acquisition. Shot and receiver spacings were 100 m, which produced 50-m CMP spacing and geometric fold of 30. The lines were processed into CRP gathers. Figure 5 shows the model overlain with raypaths to selected CRP bins for the updip line.

The CRP modeling results directly below the near vertical salt edge about 6000 m along the model (Figure 6) were selected for comparison to independent calculations. Following are the calculations for the ray with 5400 m offset (red in Figure 6). The ray reflects from the subsalt horizon at an angle of 25° (Figure 6a).

The amplitude of a ray at the receiver can be written as follows:

$$Amp_{out} = Amp_{in} * T_{12} * T_{23} * \ldots * R_t * \ldots * T_{32} * T_{21} * \text{Other Terms}$$

Where T_{mn} is the transmission coef-

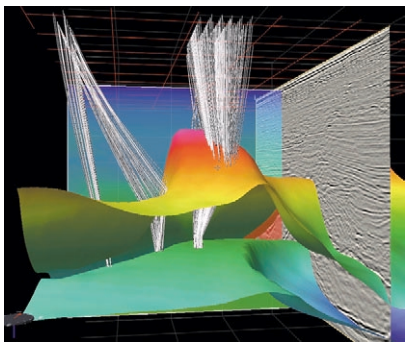

Figure 15. 3-D visualization image of raypaths to three CRP gathers on one subsalt reflection. Note focusing of rays from at least six north-south lines to area of the amplitude anomaly. 3-D visualization can be an invaluable tool in understanding imaging problems.

ficient traveling from layer m to layer n
R_t is the reflection coefficient at the reflecting horizon
Other Terms include spherical spreading, dispersion, etc.

The input amplitude (Amp_{in}) is held constant and the reflection coefficient and other terms are the same for rays traveling on the same raypath. Therefore the differences in amplitude for rays traveling in different directions in this simple model should reduce to a difference in transmission coefficients at the water bottom and the salt-sediment interfaces. The other interfaces the ray encounters in this model have no rock property contrasts and do not affect the amplitudes.

A program was written by the second author to calculate transmitted and reflected ray angles and amplitudes from Snell's law and Zoeppritz equation for specific rock properties and incident angles. Table 2 gives the rock properties for the rocks modeled. Table 3 shows the transmission coefficients and products at the interfaces. While energy is conserved at an interface, transmission coefficients can be greater than 1.0. A change in phase (for example peak to trough) in one of the resultant P- and S-rays may mean another becomes greater than 1.0 to compensate (Telford et al., 1976).

The independent calculations match within 0.2% of the ray-trace modeling results, a result that is within the modeling and round-off errors (Table 4).

The above results demonstrate that amplitude reciprocity is not correct for reflections below dipping, high-acoustic impedance interfaces. The modeling results for the entire 100-m CRP gather centered at 6000 m along the model are shown in Figure 6c. The AVO is different for lines shot in different directions, with the downdip always having smaller amplitude. The zero-offset rays should be the same because the source and receiver are coincident and the downgoing and upgoing raypaths are the same.

The velocity plotted in Figure 6c confirms that the downdip and updip paths are the same. If the paths were different, the velocity (path length divided by traveltime) would not be the same. All travel paths for the pairs of rays with switched shot and receiver are the same (raypath reciprocity), except the downdip ray with 4200-m offset. This ray goes through the near vertical edge of salt at a highly oblique angle (Figure 6a). This ray would have a small impact on the overall CRP amplitude because the transmitted amplitude is very small: i.e., most energy would be reflected or converted to shear energy at this high incidence angle.

When both the upgoing and downgoing rays penetrate the dipping salt, the shooting-direction-dependent AVO difference is greater. Figure 7 shows the raypaths and amplitudes for a CRP gather centered at 8500 m along the line. For the far offsets, updip amplitudes are twice those of downdip amplitudes.

The CRP gather results (both total amplitude and hits per bin) for the entire seismic line are plotted in Figure 8. The plot shows that the amplitude decreases under salt because much energy is reflected and converted to shear energy at the salt-sediment interfaces. The roll-on and roll-off at the edges of the model are apparent at 2000-3000 m and 11 000-12 000 m along the model. Full fold amplitude away from salt is seen at 3000-4000 m. The 1500 m near-vertical edge of salt at 6000 m causes a shadowing of the subsalt reflector. Away from this point, amplitudes increase with the exception of a fold and amplitude increase directly below the salt edge at 6000 m where the edge is undershot (compare CRPs in Figure 5).

The difference between amplitudes in downdip and updip lines is orange in Figure 9. As expected from the above reciprocity discussion, the updip line always has higher amplitude under salt. As discussed in the text and shown in Figures 6 and 7, rays with large offsets have the greatest difference in amplitude. The decrease in amplitude difference around 7000 m can then be attributed to the decrease in far-offset rays as apparent in Figure 8. Inversely, the large increase near 6000 m is the effect of an abundance of far-offset rays undershooting the near-vertical salt edge. The difference in amplitude between downdip and updip is especially large between 8500 and 10 000 m where the rays pass through the dipping salt interface twice (Figure 7).

A small part of the variation in amplitude differences is caused by hits per bin differences (blue in Figure 9). Raypaths should be reciprocal, but some are missing, usually from the updip line as shown in Figures 6 and 7. This difference appears to be an idiosyncrasy of the ray-capture algorithm in the QUIKSHOT program. It is usually a minor problem, only apparent in models having horizons with high velocity contrasts and sharp curvatures. The problem can be kept to a minimum by increasing the numbers of working rays shot.

Observations from dipping top of salt modeling include:

- Amplitude reciprocity is not correct in areas below dipping, high-impedance interfaces such as salt bodies.
- Differences in subsalt amplitudes can occur depending on shooting geometry and direction.
- Subsalt AVO response varies with shooting direction and dip of salt.
- Because of nonreciprocity of amplitudes, accurate amplitude modeling results will be obtained by replicating the shooting geometry that was used to collect the actual seismic data.
- Simple models can help interpret the idiosyncrasies of modeling programs.

Salt peaks. The impact of peaks on the top of salt and pits in the base of salt were investigated by building simple 3-D models and shooting entire 3-D surveys over them. Figure 10a shows a 3-D visualization of a model with a solitary peak projecting from a salt slab. Figure 10b is a map view of this top of salt peak, and Figure 10c is a dip map of the top salt. The peak was created by smoothing a cone shape on the top of salt horizon. Smoothing was done with a moving average smoother of 500 × 500 m (5 × 5 grid nodes). The smoother imparted a very slight noncircular element to the form apparent only in the dip map (Figure 10c). Ray

tracing simulated a marine survey with a single 8-km hydrophone cable and a 200-m offset from the source to the middle of the nearest receiver array. Distance between sources and between receivers was 200 m, producing 100-m CMPs. Spacing between lines was 100 m. The survey was shot west to east (source always east of cable). The results of the ray tracing were sorted into CRP gathers.

The CRP gather ray-trace results for the 2-km high, 3-km wide salt peak are shown in Figures 11 and 12. The fold map shows a concentration of high hits/bin directly beneath the salt peak (more than 60 fold compared to 20 fold where there is no effect of the peak). Asymmetry is apparent. First, the overall shape of the illumination disturbance is elongate in the direction of shooting caused by the linear nature of marine cable acquisition. Second, a large area of increased fold and amplitude east of the peak compared to the west is not the lack of reciprocity discussed in the last section, but rather indicates a complex 3-D interaction of the flanks of the peak with the shooting geometry.

Although there is a large fold increase under the peak, the amplitude is less than 60% of the amplitude in the area unaffected by the peak. Spreading of the rays causes the abundant rays through the peak to have greatly reduced amplitude, which is similar to the effect displayed in Figure 8 in Part 1. On a smaller scale, the area directly under the salt peak is greater than the surrounding lower amplitudes (blue). Depending on the type of amplitude equalization used in processing, this contrast could be represented as a high-amplitude anomaly. This would produce a "false" bright spot or hydrocarbon indicator, because it is the overlying salt structure that caused the amplitude variation, not the fluid in the reservoir rocks. With other salt structures and shooting geometries, the amplitude under a salt peak can increase to greater than that of the unaffected areas.

Observations from salt peak modeling include:

- Salt peaks cause the CRP amplitudes to vary in a complex pattern.
- The illumination is reduced under salt peaks, except for possible focusing areas.
- Distortion extends up to half of the maximum offset away from the structure. The distortion distance is influenced by the depth of the peak and the depth of the reflector.
- Distortion of illumination is elongate in the direction of shooting for marine acquisition geometry.
- The illumination is slightly asymmetric, with the area in the direction of the shooting from the peak having slightly higher hits per bin and amplitude.
- Salt peaks can produce "false" bright spots (HCIs).

An example of a "false" HCI found by ray-trace modeling and later tested by the drill bit was reported by Muerdter et al. (1998). Figure 13 shows two amplitude anomalies or "bright spot" clouds in 3-D prestack depth data under a salt peak in the Grand Isle South 116 (Hickory) area. The deeper anomaly is obvious on a horizon-based amplitude extraction from the 3-D prestack depth migration seismic volume (Figure 14a). Ray-trace modeling results show that a prominent hits per bin anomaly (Figure 14b) and a smaller amplitude anomaly (Figure 14c) occur at the same location as the deeper anomaly. Because the modeling results indicate salt focusing, the coincidence of the location of the deeper amplitude anomaly with the modeling amplitudes indicates that the deeper anomaly is most likely a focusing artifact, not a hydrocarbon indicator. The deeper anomaly was therefore downgraded as a prospective drilling target. The shallower amplitude anomaly, on the other hand, did not match any modeling results so it was high-graded as a prospect, was drilled, and proved to be a discovery. A sidetrack well to look updip on prospective sands in the discovery well found no pay at the deeper anomaly. Figure 15 shows raypaths to selected RPGs in the Hickory area. Note how rays from at least six north-south lines are focused into the "false" bright spot. In this case, both the peak and curved base of salt combined to focus the energy.

Next month's final part of this subsalt illumination modeling series is titled "Subsalt illumination below salt ridges and furrows and effects of acquisition orientation."

Suggested reading. "Case studies of 3-D ray-trace modeling for subsalt exploration and development in offshore Louisiana, Gulf of Mexico" by Muerdter et al. (SEG 1998 *Expanded Abstracts*). *Applied Geophysics* by Telford et al. (Cambridge, 1976). E

Corresponding author: D. Muerdter, davem@dgrc.com